ACS OMEGA

Open Access

http://pubs.acs.org/journal/acsodf

Article

Chitosan-Based Highly Sensitive Viable Humidity Sensor for Human Health Monitoring

Parvesh Kumari, Ankit Kumar, Aditya Yadav, Govind Gupta, Gaurav Gupta, Dilip D. Shivagan, and Komal Bapna*

Cite This: *ACS Omega* 2023, 8, 39511−39522

Read Online

ACCESS | Metrics & More | Article Recommendations | Supporting Information

ABSTRACT: We report a sustainable resistive-type humidity sensor based on chitosan (CS) film deposited on an interdigitated Ti/Au electrode coated SiO_2 substrate using a simple drop cast approach for human health monitoring. The sensor revealed remarkably high sensitivity (5.8 MΩ/%RH), fast response/recovery time (21 s/25 s), low hysteresis (∼9.3%), excellent reversibility, wide detecting range (11−95% RH), and high selectivity toward water vapor. The calculated associated uncertainty at different %RH indicates the excellent repeatability and stable performance of the sensor. The developed sensor is tested for different human breath patterns, and it is found that the sensor can clearly distinguish between the variations in rate and depth of respiration patterns during normal, fast, deep, and nasal breathing and can monitor for apnea-like situations. The sensor is also utilized to perform noncontact skin humidity sensing. Overall, the developed CS film humidity sensor provides a viable approach for the detection of respiratory disorders and human health issues, detected by skin moisture, in a noninvasive manner.

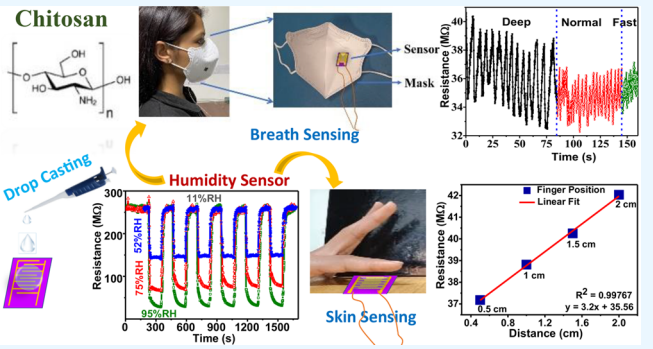

1. INTRODUCTION

Humidity sensors have become an essential component of many advanced electrical equipment monitoring systems due to their diversified applications in industrial processes, agriculture, medicine, food industry, human comfort, and environmental monitoring.[1−3] One of the most significant physiological indicators for human health care is respiratory monitoring and noncontact sensing, which may give a noninvasive approach to valuable health data and identify potential illness risks.[4,5] Recent pandemic situations like COVID-19, SARS, Ebola, etc. have further facilitated the demand for detection techniques that can operate in a noncontact way to monitor human health continuously in an isolated situation.[6,7] The humidity method is a recent technique that uses differences in the humidity level when a person inhales or exhales. Also, diseases such as diabetes, thyroid conditions, etc. affect the skin humidity conditions and hence can be identified using humidity sensors. Humidity sensors offer cheaper cost, little interference, noncontact, high sensitivity, quick reaction, and high comfort capabilities, in comparison to other health detection techniques.[8−10] Therefore, researchers are focused on developing high-performance, accurate, benign, and resource-friendly humidity sensors to monitor human respiration and skin-sensing systems under severe health conditions in real time.

A wide variety of humidity sensors have been developed using porous ceramics, semiconductors, polymeric materials, and carbon-based materials based on resistance, capacitance, impedance, optical sensors, colorimetry, quartz crystal microbalances (QCMs), and surface acoustic waves (SAWs).[11−22] Among these, polymer-based humidity sensors are extensively explored because of their numerous remarkable qualities, which include their low weight, simplicity of production, and flexibility.[23−25] Further, efforts are being made to develop high-quality humidity sensors based on natural polymers due to their nontoxicity, biocompatibility, easy functionality, and chemical inertness. Recently, Li et al. reported a silk fabric coated with a graphene oxide (GO) sensing layer fabricated by successive electroless plating of conductive interdigital electrodes and discussed its excellent humidity-sensing response.[26] Zhang et al. prepared a versatile stretchable ionic hydrogel (PTSM)-based triboelectric nanogenerator to develop a glove-based human−computer interaction system with gesture recognition and object classification potential.[27] Liu et al.

Received: July 20, 2023
Accepted: September 26, 2023
Published: October 13, 2023

reported a high-performance QCM-based humidity sensor using chitosan/polypyrrole composite to record and monitor patient respiratory patterns via an app.[28] Wang et al. designed a self-powered flexible humidity sensor using PVA/Ti_3C_2Tx nanofibers and a monolayer $MoSe_2$ piezoelectric nanogenerator, which offers high-performance humidity monitoring and energy harvesting for wearable devices.[29]

Chitosan (CS) is one of the natural polymers that emerged as a popular humidity sensor due to its additional advantage of affinity toward water molecules. CS is extracted from the exoskeleton of living organisms, shellfish, crabs, shrimp, etc. It comprises a linear chain of arbitrarily distributed β-linked D-glucosamine and N-acetyl-D-glucosamine that may be easily transformed into a hydrogel with exceptional elasticity by dispersing it in diluted organic acids like acetic acid, lactic acid, etc. The water affinity comes from the repeated functional groups like hydroxyl and amine, and these functional groups interact with water molecules through hydrogen bonding. Because of this, a large number of researchers have become interested in investigating the adsorption of water molecules by employing CS and modified CS.[30−32] Most of the reports available are based on optical techniques such as Fabry−Perot interferometers,[33] fiber Bragg grating,[30] Mach−Zehnder interferometer,[34] and QCM[35,36] and include high manufacturing costs for the sensor development and complicated detecting techniques which restrict their applications in commercial applications. In contrast to QCM and optical measurements, resistance measurements are much more straightforward, easy to set up, and cost-effective. To our knowledge, there is no report available on resistive- or capacitive-type CS-based humidity sensors. In this view, the novelty of the present work lies in developing a sustainable, cost-effective humidity sensor based on the intrinsic properties of pristine and biocompatible CS polymer (without any further modifications), with possible applications in monitoring respiration rate, skin moisture, and apnea-like situations, which have not been shown earlier.

In this paper, we report a viable CS-film-based humidity sensor with a simple drop cast method and an easy measurement setup for real-time respiratory monitoring and skin humidity detection. The sensor revealed high sensitivity to humidity changes, a broad detection range, long-term stability, and a quick response and recovery time. The associated standard uncertainty and possible sensing mechanism for the CS sensor are also discussed in the paper. The sensor was tested under various gas environments for selectivity analysis. The sensor was tested for different human breathing patterns, and it is revealed that the sensor is efficient to detect and record respiratory traits associated with different health conditions. The sensor further showed its ability to measure human skin moisture in a noncontact manner, suggesting its application in medical as well as other diverse areas.

2. EXPERIMENTAL METHODS

2.1. Preparation of Chitosan Solution. For the preparation of the CS solution, CS (≥95% deacetylation, Sigma-Aldrich), acetic acid solution (100%, Merck), ethanol (99.8%, Merck), and acetone (99.5%, Merck), were used without any further purification. To deposit the film, a 5 mg/mL concentrated solution was prepared by adding 0.5 g of CS powder into 100 mL of acetic acid (0.05 M) solution which was followed by continuous magnetic stirring at 1000 rpm for 24 h at room temperature (RT); the solution was further ultrasonicated for 20 min, which results in a yellow viscous gel solution.

2.2. Fabrication of Chitosan Film Sensor. The molecular structure and steps of fabrication of the CS film by the drop cast method are shown in Figure 1a,b. First, SiO_2 substrates were ultrasonically cleaned in acetone, ethanol, and deionized water (DI water) successively for 15 min each to remove any organic impurities from the surface of substrates. Then, interdigitated electrodes (IDEs, dimensions given in Figure 1c) of Ti/Au of 100/200 nm thickness were deposited using a thin (0.4 mm) stainless-steel mask of the desired pattern on the cleaned substrate by DC sputtering. The as-prepared CS solution is then dropped (20 μL, to cover the complete electrode area) on the IDEs coated SiO_2 substrate using a micropipet to form a CS film. The film was then dried on the hot plate at 60 °C for 20 min to improve the adhesion.

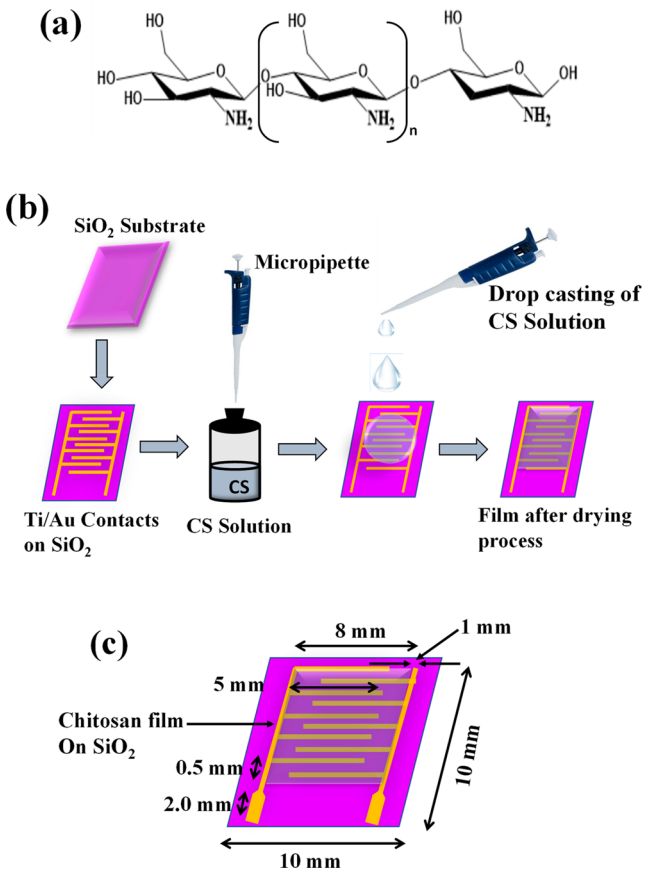

Figure 1. (a) Chemical structure of CS molecule, (b) schematic diagram of fabrication of CS film on interdigitated electrodes, and (c) developed humidity sensor with dimensions (not to scale).

2.3. Characterization and Measurements. The thickness of the film was measured to be ∼1 μm using a NanoMap 500ES Stylus profilometer. The X-ray diffraction pattern was taken by the Rigaku Tabletop Miniflex-II system using monochromatic Cu $K_{\alpha 1}$ radiation (λ = 0.15406 nm) in 2θ range from 5° to 80° with the scanning rate of 2°/min. A PerkinElmer Spectrum GX Fourier transform infrared (FTIR) system was used for determining the functional groups in the range from 400 to 4000 cm^{-1} by averaging 64 scans at a 2 cm^{-1} wavenumber resolution. The surface morphology of the film was analyzed with field emission scanning electron microscopy

https://doi.org/10.1021/acsomega.3c05244
ACS Omega 2023, 8, 39511−39522

(FESEM, TESCAN MAGNA GMH) with an accelerating voltage of 15 kV. A Keithley 2450 source meter was used for gas-sensing measurements. Hydrophilicity was determined in terms of water contact angle using a DSA 10 Mk2 drop shape analysis system.

2.4. Humidity-Sensing Measurement Setup. In the present work, we have used saturated salt solutions with known humidity values, as a source of relative humidity environment since it is an efficient, affordable, and simple method.[37,38] Different relative humidity environments were created by dissolving LiCl (RH 11%), KF (RH 33%), Mg $(NO_3)_2$ (RH 52%), NaCl (RH 75%), KBr (RH 85%), and KNO_3 (RH 95%) salts into DI water in hydrophobic rubber-capped glass containers/beakers until the salt solutions achieve their saturation state. Because some of these salt solutions are known to change their humidity values with the change in the surrounding temperature, we kept the salt solutions in a water temperature bath maintained at a constant temperature of 25 °C during all measurements. The performance of the fabricated sensor was analyzed in terms of change in the resistance at different humidity environments. The transient resistance at the intermediate state, measured by the sensor, depends on three parameters: the transferring time, data acquisition sampling rate, and the response time of the sensor. A competition between the above parameters can give rise to varying transient resistance of the sensor under different humidity conditions. A schematic diagram for the humidity-sensing setup is shown in Figure 2. A two-probe sample holder

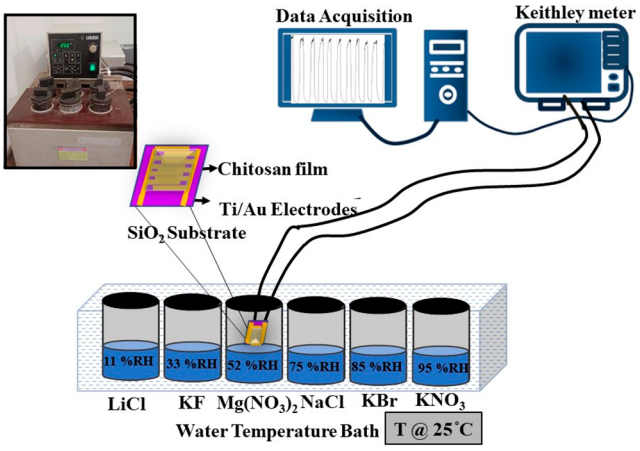

Figure 2. Schematic diagram of the humidity measurement setup. Inset shows the picture of salt solutions kept in constant-temperature water bath.

was designed for the electrical measurements. The data was processed using a Keithley Electrometer (Model No. 6517A) and a data acquisition system, which converts analog signals into digital data, and was recorded by using Kickstart software. To measure the resistance of the film with less power consumption, a low voltage of 1 V was applied. All measurements were conducted at ambient humidity (50 ± 10) %RH and RT (24 ± 2) °C conditions.

3. RESULTS AND DISCUSSION

3.1. Structural and Morphological Characteristics. The XRD result of the drop cast film is shown in Figure 3a. The phase is confirmed by the peak positions at $2\theta = 20.2°$ and 9.5° corresponding to the planes (020) and (010), (100), respectively, and the broad peak at 20.2° suggests the amorphous nature of the CS film. The FESEM image of the CS film shows a smooth, flat, and uniform surface, which suggests that the particles are arranged very close to each other in a uniform manner, as shown in Figure 3c. The FTIR spectrum (Figure 3b) shows a broad peak at 3424.74 cm^{-1} due to overlapped absorption peaks of hydroxyl (O−H) and amino (N−H) groups present in the CS chain.[39] Also, spectra show absorption peaks at 897.16 cm^{-1}, 1031.7 cm^{-1}, and 1159.27 cm^{-1}, attributed to the glycosidic bond, O−H bending vibration, and C−O−C stretching, respectively, while peaks at 2926.03 and 2860.30 cm^{-1} correspond to C−H stretching.[21] The peak at 1657.98 cm^{-1} is attributed to the C=O bond.[39] The bending deformation of the primary amine (−NH)[39] appears at approximately 1565.21 and 1422.93 cm^{-1}. The absorption peaks at 1321.01 and 1380.41 cm^{-1} correspond to C−N stretching. The band at 1159.27 and 1071.9 cm^{-1} are related to stretching of C−O−C and C−O in the chitosan ring.[39] The presence of abundant amine and hydroxyl hydrophilic functional groups in the sample indicates that CS has a good affinity toward water molecules.

After the confirmation of functional groups, the water contact angle was determined for the film surface to check the hydrophilicity of the film at the macroscopic level. A droplet (10 μL) of DI water was dropped on the surface of the CS film to measure the water contact angle, suggesting the angle to be 54.89°, as shown in Figure 3d. The water contact angle is a quantitative measurement of the wettability of the material on a solid surface. The materials having water contact angle below 90° are hydrophilic, while those above 90° are hydrophobic in nature.[25] The detected angle for the CS film demonstrates that the sample is hydrophilic and suitable for humidity-sensing measurements. Before electrical testing, all of these characterizations were performed to ensure the CS film is well-formed and suitable for humidity testing.

3.2. Humidity-Sensing Performance. For humidity-sensing measurements, we have fabricated 3 samples with the same solution keeping the identical environmental and experimental parameters. Among these, sample 3 has been used for further investigation as described in the present work (for more information, see Figure S1 in the Supporting Information). The film was placed in various relative humidity environments generated by using saturated salt solutions, as mentioned in Experimental Methods. The response/recovery time of a sensor is the amount of time it takes to alter its resistance by 90% value and is one of the key parameters for assessing a humidity sensor.[2,40,41] To measure the response-recovery time, the sensor was held in two different relative humidity conditions back-to-back with a time interval of about 120 s. The response/recovery times for the developed sensor are 8 s/17 s, 18 s/23 s, and 21 s/25 s, corresponding to humidity range from 11% RH to 52% RH, 11% RH to 75% RH, and 11% RH to 95% RH, respectively, as shown in Figure 4a. These values indicate that the sensor has fast adsorption and desorption rates toward water molecules, which is attributed to the significant adsorption functional groups on the CS film. By measuring the repeated response/recovery cycles at all RH levels, the device is further tested for its repeatability, and the pattern acquired for about 30 min is depicted in Figure 4b.

Further, sensitivity was calculated as the change in the sensing signal per unit change in relative humidity values;

https://doi.org/10.1021/acsomega.3c05244
ACS Omega 2023, 8, 39511−39522

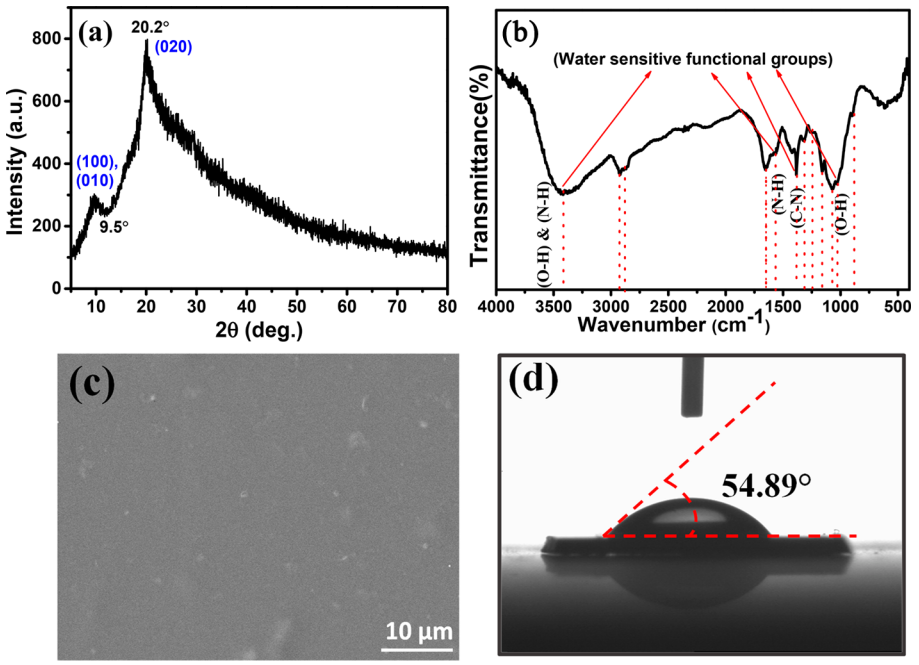

Figure 3. (a) XRD, (b) FTIR, (c) FESEM image, and (d) water contact angle measurement results.

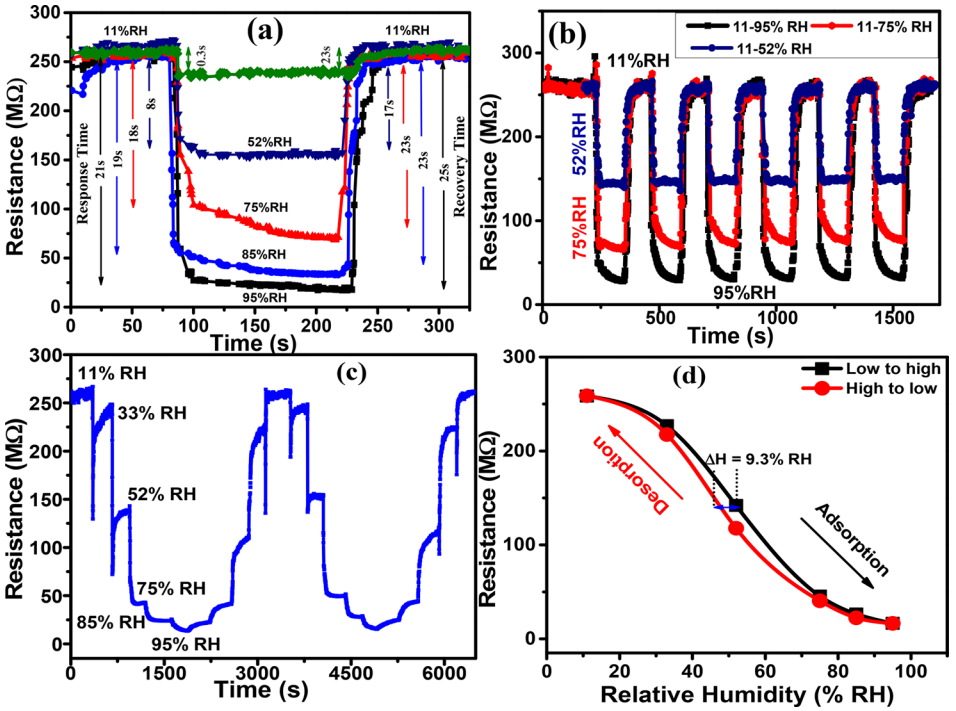

Figure 4. (a) Response and recovery time of sensor, (b) repeatability responses at different humidity values for 30 min duration, (c) typical resistance measurements in real time under gradually increasing and decreasing relative humidity between 11 and 95% RH, and (d) hysteresis curve for humidity.

$$\frac{R_0 - R_x}{\mathrm{RH}_0 - \mathrm{RH}_x}\ (\text{in } \Omega/\%\mathrm{RH})$$

where R_0 and R_x are the resistances of the device at 11% and other higher humidity levels, respectively. From Figure 4a,b, the average sensitivity of the sensor is calculated as 2.58 MΩ/%RH, while the maximum sensitivity is ∼5.8 MΩ/%RH, which is remarkably higher than most of the resistive type humidity sensors reported in previous studies.[42−46]

To determine the reliability and practical implementation of a humidity sensor, hysteresis also plays a significant role. It is defined as the difference in the resistance values of the humidity sensor at a particular % RH value during the humidification and dehumidification process.[2,40] With RH varying from 11% to 95%, we investigated the hysteresis of the CS film by a resistance ladder at each humidity level, as shown in Figure 4c. Some peaks in the signal of Figure 4c are noticed, probably due to the physical movement and the different

https://doi.org/10.1021/acsomega.3c05244
ACS Omega 2023, 8, 39511−39522

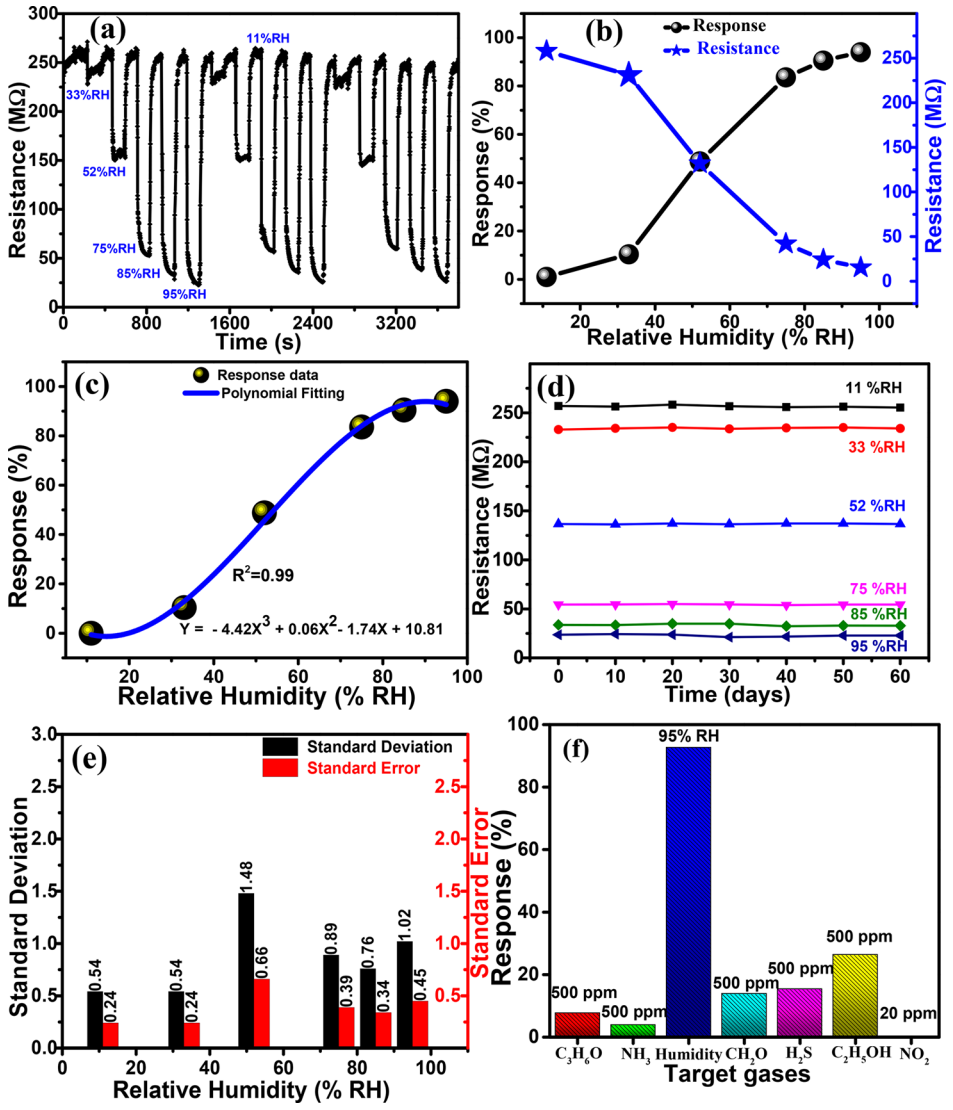

Figure 5. (a) Behavior of the fabricated sensor in repeated measurement cycles for varying relative humidity with respect to 11% RH, (b) response (%) and resistance values and its (c) polynomial fit, (d) long-term stability, (e) standard deviation and standard uncertainty at different RH, and (f) selectivity toward water molecules.

Table 1. Comparative Study of Present Work to Previously Reported Polymer-Based Resistive Type Humidity Sensors

Material	Fabrication method	Measuring Range (%RH)	Sensitivity	Response/recovery time (s)	ref.
PVDF/ZnO nanomaterials	Spin coating	5−98	3417 Ω	30/51	47
Poly (vinyl alcohol) PVA	Spin coating	7−92	−	224/56	48
Polypyrrole (PPy)-ZnO nanoparticles	Dripping technique	11−75	−	180/60	49
PLA/PANI−ZnO	Spinning	20−90	−	85/120	50
Polypyrrole (Ppy)	−	30−90	−	128/128	51
Functionalized MWCNT/HEC	Gravure press	20−80	0.0485/% RH	20/35	44
MEPTDD/CEMA	Screen-printing	20−95	0.046 log Ω/%RH	65/70	52
SnO_2/PANI	Pellet	5−95	0.22% RH^{-1}	26/30	53
PDDA/rGO	LbL self-assembly	11−97	−	108/147	40
Chitosan	Drop casting	11−95	2.58 MΩ/%RH	21/25	This work

factors governing the transient resistance (as discussed in section 2.4), during transfer of sample from one RH to another. The measured small hysteresis [adsorption (black line) and desorption (red line)] is attributed to slight differences in swelling (adsorption) and releasing (desorption) rates of the sample. The maximum hysteresis obtained by taking the average of the two cycles is about ∼9.3% near 52% RH, as plotted in Figure 4d. At high % RH values, water molecules are weakly bonded and hence may get desorbed easily, causing a lower hysteresis.

The following equation was used to calculate the sensor's % hysteresis:

https://doi.org/10.1021/acsomega.3c05244
ACS Omega 2023, 8, 39511−39522

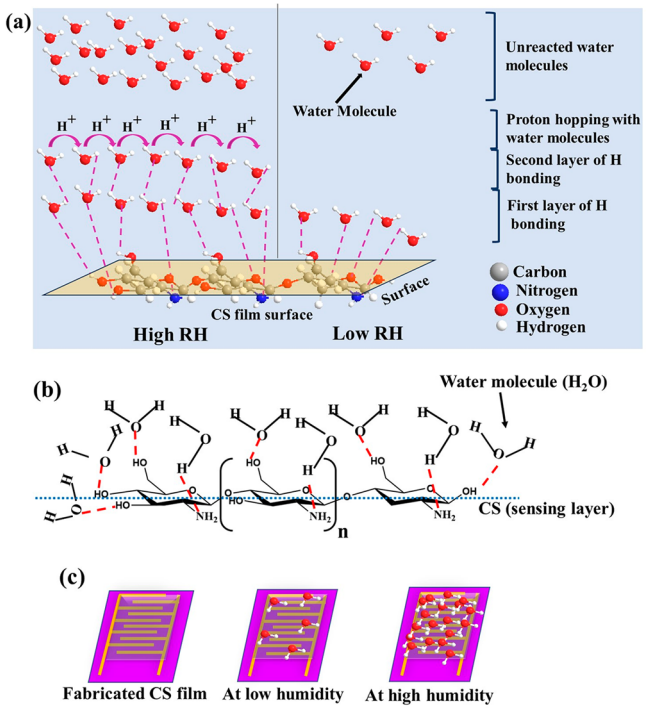

Figure 6. Sensing mechanism of humidity sensor at low and high humidity in (a) 3D model and (b) 2D model and (c) CS film at low and high humidity.

$$\text{hysteresis}\ (\%) = \frac{R_{ads} - R_{des}}{\text{sensitivity}} \times 100\% \quad (1)$$

Here, R_{ads} and R_{des} represent the resistance values of the film during the adsorption and desorption process, respectively.

Figure 5a shows the behavior of the fabricated sensor in repeated measurement cycles with varying relative humidity with respect to 11% RH. The resistance values almost restore themselves to their original values, demonstrating excellent reproducibility and reversibility of the sensor. Response, another important component of a humidity sensor is calculated as

$$\text{response}\ (\%) = \frac{R_0 - R_x}{R_0} \times 100 \quad (2)$$

To better understand the link between the sensor responses with humidity change, we plotted the graph for the sensor's response and resistance variation as a function of RH as shown in Figure 5b. The sensor reveals a cubic polynomial fit, $y = -4.42x^3 + 0.06x^2 - 1.74x + 10.81$ with the change in RH as shown in Figure 5c, with a correlation coefficient of $R^2 = 0.99$. This suggests that although the sensor responds to all humidity ranges, it is more sensitive toward the mid-humidity change. This study has been performed for a RT humidity sensor. To see the effect of temperature variation on the humidity-sensing properties, we examined the resistance change of the sensor with temperatures ranging from 20 to 30 °C at 50% RH. It is revealed that the change in resistance values with temperature shows a linear trend with $R^2 = 0.99$ fitted with a linear equation $y = 240.3 - 3.8x$ (for more information, see supporting note 3 in the Supporting Information). The sensor's stability was checked by measuring its resistance at each humidity value ranging from 11% to 95% in an interval of 10 days, monitored for 60 days. The sensor exhibits only a slight fluctuation in resistance, suggesting long-term stability and a high-quality film with excellent uniformity.

Further, the reliability and precision of any measurement are evaluated using standard deviation and uncertainty calculations. Standard deviation (σ) is the measure of the degree of randomness of a repeated measurement, whereas standard uncertainty (SU) specifies the uncertainty in the average measured value. Figure 5e shows these calculated values at different humidity ranges. The standard deviation for the developed sensor is calculated from the mean of the 5 measured values corresponding to each specified RH level, as given in the formula

$$\sigma = \sqrt{\frac{\sum (x_i - \mu)^2}{N - 1}} \quad (3)$$

where N is the number of measurements, x_i is the individual value, and μ is the average value. The standard uncertainty or type-A uncertainty due to measurement repeatability is calculated as

$$\text{SU} = \frac{\sigma}{\sqrt{N}} \quad (4)$$

As shown in Figure 5e, the maximum standard uncertainty was thus obtained to be ±0.78 MΩ for the measured resistance value of 72 MΩ at 75% RH. The nominal standard uncertainty in the given humidity range suggests acceptable repeatability and stable performance of the CS sensor. The sensor's selectivity test was also performed for volatile organic compounds (VOCs) and other gases at ambient temperature. It is seen that the sensor is highly selective toward water vapors as compared to its surroundings' interference gases, demonstrating its favorable applicability as a humidity sensor. For NO_2 (20 ppm) no response was observed, and only small responses of 13.8%, 3.8%, 7.6%, and 15.3% for formaldehyde, ammonia, acetone, and H_2S vapors, respectively, were measured at 500 ppm in comparison of humidity (92.7%). Even for water-soluble ethanol, the sensor only responds by 26.3%, ruling out the interference of other gases when used as a humidity sensor. In Table 1 we have compared the present work to the earlier reported polymer-based resistive type humidity sensors. It is revealed that the results of the present work are superior in many aspects as presented in Table 1.

3.3. Humidity-Sensing Mechanism. The above results show that CS has commendable humidity-sensing properties. This is mainly due to the presence of several repeating hydrophilic functional groups such as amines and hydroxyls in the CS which are capable of forming hydrogen bonding with water molecules present in the environment.[54] Some of the amino groups presented in CS get protonated during the acetic acid treatment,[54,55] as shown in eq 5. The nitrogen in the amino/deprotonated amino group forms a hydrogen bond with the hydrogen of the water molecules, and the hydrogen present in the hydroxyl group makes a hydrogen bond with the oxygen of the water molecules present in the atmosphere.[36,56] As the hydrogen bond is weak, they are responsible for the reversible adsorption and desorption process of water molecules on the surface of the CS film, depending on the relative humidity content in the atmosphere.

$$RNH_2 + CH_3COOH \rightarrow RNH_3^+ + CH_3COO^- \quad (5)$$

$$RNH_3^+ + H_2O \rightarrow RNH_2 + H_3O^+ \quad (6)$$

https://doi.org/10.1021/acsomega.3c05244
ACS Omega 2023, 8, 39511−39522

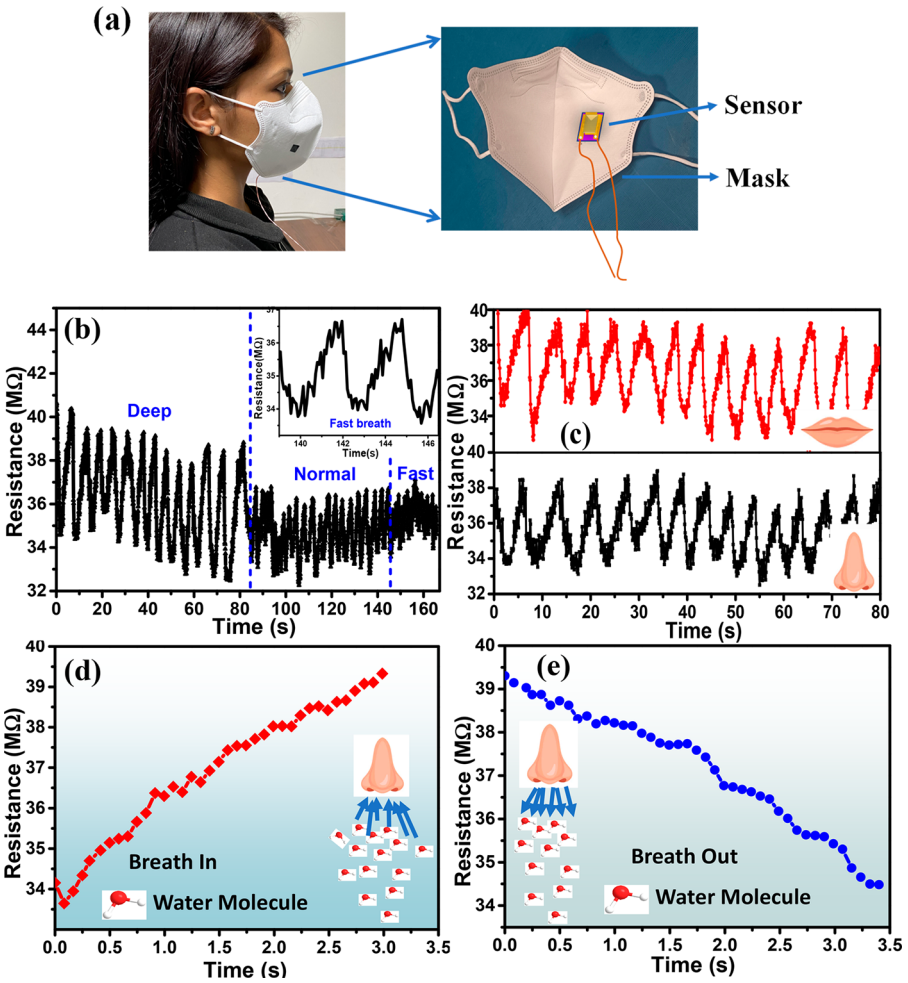

Figure 7. (a) Respiratory monitoring test and (b) humidity response of the CS sensor under different breath monitoring rates (deep, normal, and fast breath). (c) Comparison of nose and mouth breathing monitoring intensity. (d and e) Response graph for nose breathing (during breath-in and breath-out).

$$H_2O + H_3O^+ \rightarrow H_3O^+ + H_2O \quad (7)$$

To demonstrate the mechanism of the film, we present a model of water molecules adsorbed on its surface in 3D and 2D models, as illustrated in Figure 6a,b. When water comes in contact with the surface of the CS film, protonated NH_2 groups release one H^+ ion as given in eq 6. At low humidity levels, the H^+ ions are released due to the dissociation of water molecules under the application of electric field, and these H^+ ions hop through nearby water molecules and NH^{3+} ions. Due to the lower concentration of water molecules at low RH, proton migration is difficult due to breakages in conduction paths, leading to a high resistance. Over a certain threshold, more water molecules form hydrogen bonds with the water molecules adsorbed on the CS surface. With the increase in humidity, there is a multilayer physisorption of water molecules adhered by weak hydrogen bonding forming a continuous water layer on the CS surface[57] as presented in Figure 6a. These molecules when ionized from hydronium ions (H_3O^+) act as high mobility charge carriers at high humidity. Hence, according to the Grotthuss mechanism (eq 7), it leads to an increase in the electrical conductivity. As a result, the resistance drops down remarkably as humidity rises. Conversely, their contribution to the swelling phenomenon of CS in the high-humidity environment to a certain extent is negligible, resulting in a lower humidity hysteresis. The interaction of the water molecules with the surface of the sensor at different humidity levels is shown in Figure 6c.

3.4. Applications in Respiratory Monitoring. The exhaled air in human breath contains a particular amount of humidity level, and hence, environmental change around the nose and mouth area during breathing includes vital information about human health-related concerns. Humidity sensing is an easy-to-use and effective noninvasive way to assess a person's health issues. In recent years, especially after the COVID-19 pandemic, humidity sensors have attracted researchers' interest for this purpose. A type of pulmonary humidity sensor based on ionic conductive metal−organic frameworks was developed by Zhang et al. and has shown applications in flexible electronics, noncontact sensing, and everyday life humidity detection.[58] Choi et al. reported real-time breath monitoring based on 2D layered Mn and Ru nanosheets by integrating Ru oxide nanostructure.[59] Liu et al. have shown CS/polypyrrole composite QCM sensor prepared by a facile physical modification method and demonstrated its response to different breathing patterns.[28] Dia et al. describe a polyelectrolyte-based humidity sensor, in situ cross-linked on the substrate printed with IDEs that shows an extremely quick response time and can be used for monitoring respiration.[60] Ullah et al. reported a highly sensitive, flexible, and eco-friendly

https://doi.org/10.1021/acsomega.3c05244
ACS Omega 2023, 8, 39511−39522

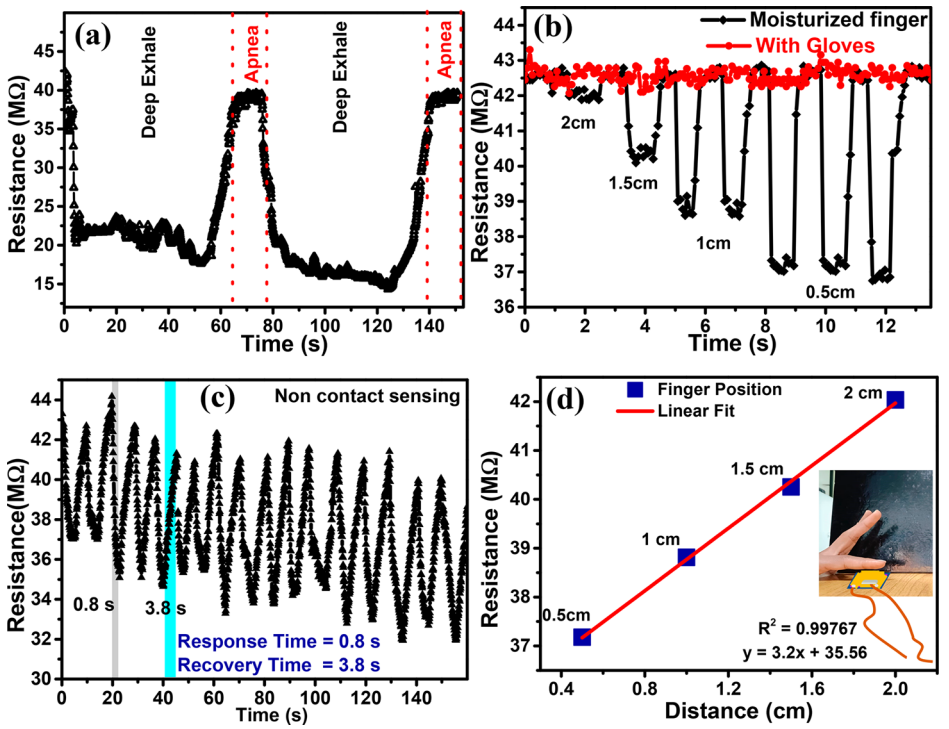

Figure 8. Real-time response of the sensor for (a) breath and apnea-like conditions, (b) contactless skin humidity with gloves and without gloves, (c) response/recovery time for moisturized figure with constant distance, and (d) sensors' response at various distance from a moisturized finger.

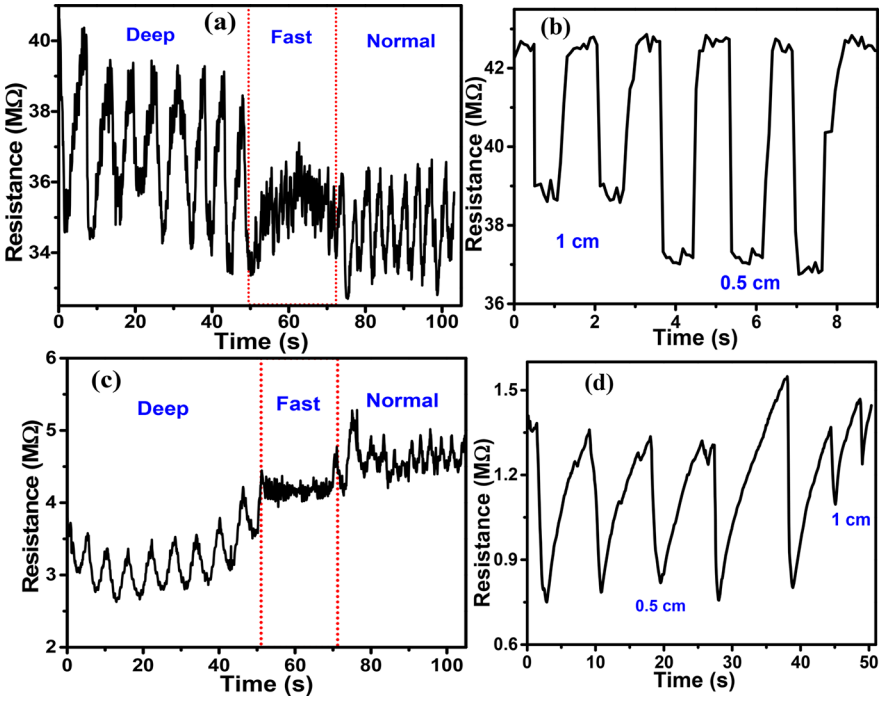

Figure 9. Comparative analysis of breath monitoring and noncontact sensing characteristics of the (a and b) fabricated sensor and (c and d) commercial humidity sensor.

biodegradable nonwoven paper-based humidity sensor on polyethylene terephthalate (PET) substrate with copper tape as electrodes and demonstrated its applications in health and medicine.[61] In recent work, Li et al. proposed a flexible humidity sensor based on alkalized MXenes and polydopamine for human−machine interaction in a noncontact manner.[62] Such studies suggest the emerging application of humidity sensors in determining human health severities related to respiration and skin moisture.

To investigate the application of the CS humidity sensor in breathing, the sensor is attached to an N95 mask using adhesive tape (Figure 7a) and its response is studied in different artificially created breath pattens. The breathing rates of 8, 11, and 20 breaths per minute (bpm) for deep, normal,

https://doi.org/10.1021/acsomega.3c05244
ACS Omega 2023, 8, 39511−39522

and fast breaths were observed, respectively, as shown in Figure 7b. Additionally, it is possible to see a distinct difference in peak timings for deep breathing (7.8 s), normal breathing (5.4 s), and fast breathing (2.9 s). The observed variation in electric signal patterns during different rates reveals the ability of the sensor to differentiate between a person's various physical states.

In deep breathing, the intensity of signals becomes higher and the rate becomes less as compared to normal and fast breathing. The amplitude variation under slow breathing is approximately 1.44 times higher than that during medium breathing and 2.68 times higher than that during fast breathing. In addition, fast breathing leads to high frequency and low amplitude in resistance signals because of the limited water molecule concentration. From Figure 7d,e we can understood that the observed decrease in the resistance during exhalation and an increase in resistance during inhalation are consistent with the sensor response for the humidity change in the near environment. Nasal breathing is the preferred method in common situations; however mouth breathing is sometimes used in some typical situations like during heavy activity, nasal congestion caused by a cold, etc. Therefore, we have considered monitoring of breathing rate, purposefully performed by mouth as well as nasal and plotted in Figure 7c. The difference in the intensity of mouth and nose breathing can be seen, which is due to the presence of saliva and moisture in mouth-exhaled air.

In other applications of the sensor to identify sleep apnea (a serious sleep condition where breathing repeatedly stops and starts), it is essential to regularly monitor breathing during sleep. Therefore, the patterns were recorded for apnea-like situations where the breath was purposely stopped for a short duration. In Figure 8a the difference between apnea and deep exhale conditions is shown. When breath suddenly stops in the apnea condition, humidity surrounding the sensor suddenly goes down, increasing the resistance, while the sensor shows a decrease in resistance during the breath out. The above results suggest that a reliable humidity sensor can be a good choice to speculate about any breakdown condition related to breath patterns such as asthma and apnea and contagious diseases such as COVID-19, etc. For the practical use of the sensor, we assessed the sensor's performance by positioning it at various locations within the mask, which had no influence on its detection capability.

To further investigate the CS humidity sensor's ability to detect human skin surface humidity in a noncontact manner, the sensor is exposed to fingers with different conditions, one which is specially moisturized and the another which is wearing a glove, and placed at various heights varying from 0.5 to 2 cm, as illustrated in the inset of Figure 8d. The resistance is observed to decrease when the moisturized finger gets closer to the CS humidity sensor while the response remains constant for the finger with glove, as shown in Figure 8b. When the moisturized finger approaches the sensor, there is a noticeable increase in resistance, with response and recovery time of 0.8 s/3.8 s (Figure 8c). The resistance response of the sensor film as a function of distance between the human finger and sensor is fitted with a linear equation, $y = 3.2x + 35.56$, suggesting a good fit with a high correlation coefficient $R^2 = 0.99767$. It depicts that the sensor is able to detect the skin humidity in a linear manner with respect to increase in the distance between the human finger and sensor (0.5−2 cm), as shown in Figure 8d.

To further check the reliability of the developed CS sensor, its breath monitoring and noncontact sensing properties were compared to those of a commercial sensor, as shown in Figure 9a−d. The findings suggest that the fabricated sensor can perform better for the human health study (for more information, see supporting note 1 in the Supporting Information). Atopic dermatitis, diabetes, thyroid, or kidney diseases which are reflected in human skin humidity conditions can be diagnosed by humidity sensors in a noncontact manner.[63] According to the above results, the CS film humidity sensor may be an effective way to quickly monitor human health issues by sensing the change in skin humidity and breathing patterns in real time.

4. CONCLUSIONS

In conclusion, we have developed a resistive type humidity sensor made of natural polymer CS by using a simple drop cast technique for human health monitoring. The sample was characterized with X-ray diffraction, scanning electron microscopy, and FTIR spectroscopy and for its hygroscopic nature. The humidity-sensing properties were investigated in the range of 11−95% RH in terms of the resistance change, which revealed fast response/recovery time, remarkably high sensitivity, low hysteresis, and good water vapor selectivity. The nominal value of standard uncertainty indicates the excellent repeatability and stable performance of the sensor. The CS film sensor could accurately differentiate the rates and depth of real-time respiration patterns and could track skin humidity variations. The remarkable humidity-sensing properties, respiratory and skin sensing response, nontoxicity, and low cost of the developed CS humidity sensor provide a viable solution for the early detection of many human health problems in a noninvasive manner. The detection of the smallest RH variations on human skin in a noncontact manner reveals another prospect for future technology based on intelligent touchless switches and displays. The study further demands transformation of these sensors into smart wireless, self-powered humidity sensors with AI and advanced technology support for such sophisticated applications.

■ ASSOCIATED CONTENT

Supporting Information

The Supporting Information is available free of charge at https://pubs.acs.org/doi/10.1021/acsomega.3c05244.

Comparative analysis of breath monitoring and noncontact sensing characteristics of the fabricated sensor and commercial humidity sensor; batch study and standard deviation at different %RH of fabricated sensor; temperature-dependent study of CS film sensor at 50% RH (PDF)

■ AUTHOR INFORMATION

Corresponding Author

Komal Bapna − *Temperature and Humidity Metrology, CSIR-National Physical Laboratory, New Delhi 110012, India; Academy of Scientific & Innovative Research (AcSIR), Ghaziabad 201002, India;* orcid.org/0000-0001-5358-7309; Email: komal.bapna@nplindia.org

Authors

Parvesh Kumari − *Temperature and Humidity Metrology, CSIR- National Physical Laboratory, New Delhi 110012,*

https://doi.org/10.1021/acsomega.3c05244
ACS Omega 2023, 8, 39511−39522

India; Academy of Scientific & Innovative Research (AcSIR), Ghaziabad 201002, India

Ankit Kumar − *Temperature and Humidity Metrology, CSIR-National Physical Laboratory, New Delhi 110012, India; Academy of Scientific & Innovative Research (AcSIR), Ghaziabad 201002, India*

Aditya Yadav − *Sensor Devices and Metrology, CSIR-National Physical Laboratory, New Delhi 110012, India; Academy of Scientific & Innovative Research (AcSIR), Ghaziabad 201002, India*

Govind Gupta − *Sensor Devices and Metrology, CSIR-National Physical Laboratory, New Delhi 110012, India; Academy of Scientific & Innovative Research (AcSIR), Ghaziabad 201002, India*

Gaurav Gupta − *Temperature and Humidity Metrology, CSIR- National Physical Laboratory, New Delhi 110012, India*

Dilip D. Shivagan − *Temperature and Humidity Metrology, CSIR- National Physical Laboratory, New Delhi 110012, India; Academy of Scientific & Innovative Research (AcSIR), Ghaziabad 201002, India*

Complete contact information is available at: https://pubs.acs.org/10.1021/acsomega.3c05244

Notes

The authors declare no competing financial interest.

■ ACKNOWLEDGMENTS

The authors would like to thank Prof. Venu Gopal Achanta, Director, CSIR-NPL, and Dr. Nita Dilawar, Head of Physico-Mechanical Metrology for their constant support and encouragement. We acknowledge Dr. Ajeet Kumar for helping in depositing Au/Ti IDEs on the SiO_2 substrate. Mr. Sumit, Dr. Jai Tawale, Dr. Vikas, and Mr. Mukul are acknowledged for XRD, FESEM, water contact angle, and FTIR measurements. We thank our colleagues Dr. Umesh Pant, Hansraj Meena, Ashish Bhatt, and Saroj from Temperature and Humidity Metrology for their help during this work. Ms. Parvesh acknowledges UGC, New Delhi, for senior research fellowship award.

■ REFERENCES

(1) Farahani, H.; Wagiran, R.; Hamidon, M. Humidity Sensors Principle, Mechanism, and Fabrication Technologies: A Comprehensive Review. *Sensors* **2014**, *14* (5), 7881−7939.

(2) Kumar, A.; Gupta, G.; Bapna, K.; Shivagan, D. D. Semiconductor-Metal-Oxide-Based Nano-Composites for Humidity Sensing Applications. *Mater. Res. Bull.* **2023**, *158*, 112053.

(3) Li, Z.; Zhang, H.; Zheng, W.; Wang, W.; Huang, H.; Wang, C.; MacDiarmid, A. G.; Wei, Y. Highly Sensitive and Stable Humidity Nanosensors Based on LiCl Doped TiO_2 Electrospun Nanofibers. *J. Am. Chem. Soc.* **2008**, *130* (15), 5036−5037.

(4) Nicolò, A.; Massaroni, C.; Schena, E.; Sacchetti, M. The Importance of Respiratory Rate Monitoring: From Healthcare to Sport and Exercise. *Sensors* **2020**, *20* (21), 6396.

(5) Zhang, J.; Wang, X.-X.; Zhang, B.; Ramakrishna, S.; Yu, M.; Ma, J.-W.; Long, Y.-Z. In Situ Assembly of Well-Dispersed Ag Nanoparticles throughout Electrospun Alginate Nanofibers for Monitoring Human Breath—Smart Fabrics. *ACS Appl. Mater. Interfaces* **2018**, *10* (23), 19863−19870.

(6) Massaroni, C.; Nicolò, A.; Schena, E.; Sacchetti, M. Remote Respiratory Monitoring in the Time of COVID-19. *Front. Physiol.* **2020**, *11*, 635.

(7) Zhang, H.; Zhang, D.; Zhang, B.; Wang, D.; Tang, M. Wearable Pressure Sensor Array with Layer-by-Layer Assembled MXene Nanosheets/Ag Nanoflowers for Motion Monitoring and Human-Machine Interfaces. *ACS Appl. Mater. Interfaces* **2022**, *14* (43), 48907−48916.

(8) Duan, Z.; Jiang, Y.; Tai, H. Recent Advances in Humidity Sensors for Human Body Related Humidity Detection. *J. Mater. Chem. C* **2021**, *9* (42), 14963−14980.

(9) An, J.; Le, T.-S. D.; Huang, Y.; Zhan, Z.; Li, Y.; Zheng, L.; Huang, W.; Sun, G.; Kim, Y.-J. All-Graphene-Based Highly Flexible Noncontact Electronic Skin. *ACS Appl. Mater. Interfaces* **2017**, *9* (51), 44593−44601.

(10) Zhang, D.; Wang, M.; Tang, M.; Song, X.; Zhang, X.; Kang, Z.; Liu, X.; Zhang, J.; Xue, Q. Recent Progress of Diversiform Humidity Sensors Based on Versatile Nanomaterials and Their Prospective Applications. *Nano Res.* **2022**, DOI: 10.1007/s12274-022-4917-y.

(11) Smith, A. D.; Elgammal, K.; Niklaus, F.; Delin, A.; Fischer, A. C.; Vaziri, S.; Forsberg, F.; Råsander, M.; Hugosson, H.; Bergqvist, L.; Schröder, S.; Kataria, S.; Östling, M.; Lemme, M. C. Resistive Graphene Humidity Sensors with Rapid and Direct Electrical Readout. *Nanoscale* **2015**, *7* (45), 19099−19109.

(12) Dai, H.; Feng, N.; Li, J.; Zhang, J.; Li, W. Chemiresistive Humidity Sensor Based on Chitosan/Zinc Oxide/Single-Walled Carbon Nanotube Composite Film. *Sens. Actuators, B* **2019**, *283*, 786−792.

(13) Kim, E.; Kim, S. Y.; Jo, G.; Kim, S.; Park, M. J. Colorimetric and Resistive Polymer Electrolyte Thin Films for Real-Time Humidity Sensors. *ACS Appl. Mater. Interfaces* **2012**, *4* (10), 5179−5187.

(14) Park, S. Y.; Kim, Y. H.; Lee, S. Y.; Sohn, W.; Lee, J. E.; Kim, D. H.; Shim, Y.-S.; Kwon, K. C.; Choi, K. S.; Yoo, H. J.; Suh, J. M.; Ko, M.; Lee, J.-H.; Lee, M. J.; Kim, S. Y.; Lee, M. H.; Jang, H. W. Highly Selective and Sensitive Chemoresistive Humidity Sensors Based on RGO/MoS_2 van Der Waals Composites. *J. Mater. Chem. A* **2018**, *6* (12), 5016−5024.

(15) Chani, M. T. S. Impedimetric Sensing of Temperature and Humidity by Using Organic-Inorganic Nanocomposites Composed of Chitosan and a CuO-Fe3O4 Nanopowder. *Microchim Acta* **2017**, *184* (7), 2349−2356.

(16) Chani, M. T. S. Fabrication and Characterization of Chitosan-CeO2-CdO Nanocomposite Based Impedimetric Humidity Sensors. *Int. J. Biol. Macromol.* **2022**, *194*, 377−383.

(17) Feng, Y.; Gong, S.; Du, E.; Yu, K.; Ren, J.; Wang, Z.; Zhu, Z. TaS_2 Nanosheet-Based Ultrafast Response and Flexible Humidity Sensor for Multifunctional Applications. *J. Mater. Chem. C* **2019**, *7* (30), 9284−9292.

(18) Voznesenskiy, S. S.; Sergeev, A. A.; Mironenko, A. Yu.; Bratskaya, S. Yu.; Kulchin, Yu. N. Integrated-Optical Sensors Based on Chitosan Waveguide Films for Relative Humidity Measurements. *Sens. Actuators, B* **2013**, *188*, 482−487.

(19) Tang, Y.; Li, Z.; Ma, J.; Wang, L.; Yang, J.; Du, B.; Yu, Q.; Zu, X. Highly Sensitive Surface Acoustic Wave (SAW) Humidity Sensors Based on Sol-Gel SiO2 Films: Investigations on the Sensing Property and Mechanism. *Sens. Actuators, B* **2015**, *215*, 283−291.

(20) Le, X.; Wang, X.; Pang, J.; Liu, Y.; Fang, B.; Xu, Z.; Gao, C.; Xu, Y.; Xie, J. A High Performance Humidity Sensor Based on Surface Acoustic Wave and Graphene Oxide on AlN/Si Layered Structure. *Sens. Actuators, B* **2018**, *255*, 2454−2461.

(21) Chen, W.; Chen, B.; Lv, R.; Wu, M.; Zhou, J.; Lu, B.; Huang, B.; Lu, Q.; Tang, L. Fabrication of Quartz Crystal Microbalance Humidity Sensors Based on Super-Hydrophilic Cellulose Nanocrystals. *Cellulose* **2021**, *28* (6), 3409−3421.

(22) Momtaz, M.; Chen, J. High-Performance Colorimetric Humidity Sensors Based on Konjac Glucomannan. *ACS Appl. Mater. Interfaces* **2020**, *12* (48), 54104−54116.

(23) Najeeb, M. A.; Ahmad, Z.; Shakoor, R. A. Organic Thin-Film Capacitive and Resistive Humidity Sensors: A Focus Review. *Adv. Mater. Interfaces* **2018**, *5* (21), 1800969.

(24) Lu, Y.; Yang, G.; Shen, Y.; Yang, H.; Xu, K. Multifunctional Flexible Humidity Sensor Systems Towards Noncontact Wearable Electronics. *Nano-Micro Lett.* **2022**, *14* (1), 150.
(25) Duan, Z.; Jiang, Y.; Yan, M.; Wang, S.; Yuan, Z.; Zhao, Q.; Sun, P.; Xie, G.; Du, X.; Tai, H. Facile, Flexible, Cost-Saving, and Environment-Friendly Paper-Based Humidity Sensor for Multifunctional Applications. *ACS Appl. Mater. Interfaces* **2019**, *11* (24), 21840−21849.
(26) Li, B.; Xiao, G.; Liu, F.; Qiao, Y.; Li, C. M.; Lu, Z. A Flexible Humidity Sensor Based on Silk Fabrics for Human Respiration Monitoring. *J. Mater. Chem. C* **2018**, *6* (16), 4549−4554.
(27) Zhang, H.; Zhang, D.; Wang, Z.; Xi, G.; Mao, R.; Ma, Y.; Wang, D.; Tang, M.; Xu, Z.; Luan, H. Ultrastretchable, Self-Healing Conductive Hydrogel-Based Triboelectric Nanogenerators for Human-Computer Interaction. *ACS Appl. Mater. Interfaces* **2023**, *15* (4), 5128−5138.
(28) Liu, X.; Zhang, D.; Wang, D.; Li, T.; Song, X.; Kang, Z. A Humidity Sensing and Respiratory Monitoring System Constructed from Quartz Crystal Microbalance Sensors Based on a Chitosan/Polypyrrole Composite Film. *J. Mater. Chem. A* **2021**, *9* (25), 14524−14533.
(29) Wang, D.; Zhang, D.; Li, P.; Yang, Z.; Mi, Q.; Yu, L. Electrospinning of Flexible Poly(Vinyl Alcohol)/MXene Nanofiber-Based Humidity Sensor Self-Powered by Monolayer Molybdenum Diselenide Piezoelectric Nanogenerator. *Nano-Micro Lett.* **2021**, *13* (1), 57.
(30) D'Amato, R.; Polimadei, A.; Terranova, G.; Caponero, M. A. Humidity Sensing by Chitosan-Coated Fibre Bragg Gratings (FBG). *Sensors* **2021**, *21* (10), 3348.
(31) Zou, J.; Zhang, K.; Zhang, Q. Giant Humidity Response Using a Chitosan-Based Protonic Conductive Sensor. *IEEE Sensors J.* **2016**, *16* (24), 8884−8889.
(32) Chen, L. H.; Li, T.; Chan, C. C.; Menon, R.; Balamurali, P.; Shaillender, M.; Neu, B.; Ang, X. M.; Zu, P.; Wong, W. C.; Leong, K. C. Chitosan Based Fiber-Optic Fabry-Perot Humidity Sensor. *Sens. Actuators, B* **2012**, *169*, 167−172.
(33) Shrivastav, A. M.; Gunawardena, D. S.; Liu, Z.; Tam, H.-Y. Microstructured Optical Fiber Based Fabry-Pérot Interferometer as a Humidity Sensor Utilizing Chitosan Polymeric Matrix for Breath Monitoring. *Sci. Rep* **2020**, *10* (1), 6002.
(34) Ni, K.; Chan, C. C.; Chen, L.; Dong, X.; Huang, R.; Ma, Q. A Chitosan-Coated Humidity Sensor Based on Mach-Zehnder Interferometer with Waist-Enlarged Fusion Bitapers. *Optical Fiber Technology* **2017**, *33*, 56−59.
(35) Qi, P.; Xu, Z.; Zhang, T.; Fei, T.; Wang, R. Chitosan Wrapped Multiwalled Carbon Nanotubes as Quartz Crystal Microbalance Sensing Material for Humidity Detection. *J. Colloid Interface Sci.* **2020**, *560*, 284−292.
(36) Qi, P.; Xu, Z.; Zhou, T.; Zhang, T.; Zhao, H. Study on a Quartz Crystal Microbalance Sensor Based on Chitosan-Functionalized Mesoporous Silica for Humidity Detection. *J. Colloid Interface Sci.* **2021**, *583*, 340−350.
(37) Carr, D. S.; Harris, B. L. Solutions for Maintaining Constant Relative Humidity. *Ind. Eng. Chem.* **1949**, *41* (9), 2014−2015.
(38) Greenspan, L. Humidity Fixed Points of Binary Saturated Aqueous Solutions. *J. RES. NATL. BUR. STAN. SECT. A* **1977**, *81A* (1), 89.
(39) Zhang, K.; Hu, R.; Fan, G.; Li, G. Graphene Oxide/Chitosan Nanocomposite Coated Quartz Crystal Microbalance Sensor for Detection of Amine Vapors. *Sens. Actuators, B* **2017**, *243*, 721−730.
(40) Zhang, D.; Tong, J.; Xia, B.; Xue, Q. Ultrahigh Performance Humidity Sensor Based on Layer-by-Layer Self-Assembly of Graphene Oxide/Polyelectrolyte Nanocomposite Film. *Sens. Actuators, B* **2014**, *203*, 263−270.
(41) Yadav, B. C.; Sikarwar, S.; Yadav, R.; Chaudhary, P.; Dzhardimalieva, G. I.; Golubeva, N. D. Preparation of Zinc (II) Nitrate Poly Acryl Amide (PAAm) and Its Optoelectronic Application for Humidity Sensing. *J. Mater. Sci: Mater. Electron* **2018**, *29* (9), 7770−7777.
(42) Adib, M. R.; Lee, Y.; Kondalkar, V. V.; Kim, S.; Lee, K. A Highly Sensitive and Stable RGO:MoS_2 -Based Chemiresistive Humidity Sensor Directly Insertable to Transformer Insulating Oil Analyzed by Customized Electronic Sensor Interface. *ACS Sens.* **2021**, *6* (3), 1012−1021.
(43) Yu, S.; Zhang, H.; Chen, C.; Zhang, J.; Li, P. Preparation and Mechanism Investigation of Highly Sensitive Humidity Sensor Based on Two-Dimensional Porous Gold/Graphite Carbon Nitride Nanoflake. *Sens. Actuators, B* **2020**, *307*, 127679.
(44) Turkani, V. S.; Maddipatla, D.; Narakathu, B. B.; Saeed, T. S.; Obare, S. O.; Bazuin, B. J.; Atashbar, M. Z. A Highly Sensitive Printed Humidity Sensor Based on a Functionalized MWCNT/HEC Composite for Flexible Electronics Application. *Nanoscale Adv.* **2019**, *1* (6), 2311−2322.
(45) Siddiqui, G. U.; Sajid, M.; Ali, J.; Kim, S. W.; Doh, Y. H.; Choi, K. H. Wide Range Highly Sensitive Relative Humidity Sensor Based on Series Combination of MoS2 and PEDOT:PSS Sensors Array. *Sens. Actuators, B* **2018**, *266*, 354−363.
(46) Parthibavarman, M.; Hariharan, V.; Sekar, C. High-Sensitivity Humidity Sensor Based on SnO2 Nanoparticles Synthesized by Microwave Irradiation Method. *Materials Science and Engineering: C* **2011**, *31* (5), 840−844.
(47) Arularasu, M. V.; Harb, M.; Vignesh, R.; Rajendran, T. V.; Sundaram, R. PVDF/ZnO Hybrid Nanocomposite Applied as a Resistive Humidity Sensor. *Surfaces and Interfaces* **2020**, *21*, 100780.
(48) Karunarathne, T. S. E. F.; Wijesinghe, W. P. S. L.; Rathuwadu, N. P. W.; Karalasingam, A.; Manoharan, N.; Sameera, S. A. L.; Sandaruwan, C.; Amaratunga, G. A.; De Silva, S. G. M. Fabrication and Characterization of Partially Conjugated Poly (Vinyl Alcohol) Based Resistive Humidity Sensor. *Sensors and Actuators A: Physical* **2020**, *314*, 112263.
(49) Najjar, R.; Nematdoust, S. A Resistive-Type Humidity Sensor Based on Polypyrrole and ZnO Nanoparticles: Hybrid Polymers Vis-a-Vis Nanocomposites. *RSC Adv.* **2016**, *6* (113), 112129−112139.
(50) Parangusan, H.; Bhadra, J.; Ahmad, Z.; Mallick, S.; Touati, F.; Al-Thani, N. Humidity Sensor Based on Poly(Lactic Acid)/PANI-ZnO Composite Electrospun Fibers. *RSC Adv.* **2021**, *11* (46), 28735−28743.
(51) Hussain, M.; Hasnain, S.; Khan, N. A.; Bano, S.; Zuhra, F.; Ali, M.; Khan, M.; Abbas, N.; Ali, A. Design and Fabrication of a Fast Response Resistive-Type Humidity Sensor Using Polypyrrole (Ppy) Polymer Thin Film Structures. *Polymers* **2021**, *13* (18), 3019.
(52) Lim, D.-I.; Cha, J.-R.; Gong, M.-S. Preparation of Flexible Resistive Micro-Humidity Sensors and Their Humidity-Sensing Properties. *Sens. Actuators, B* **2013**, *183*, 574−582.
(53) Shukla, S. K.; Shukla, S. K.; Govender, P. P.; Agorku, E. S. A Resistive Type Humidity Sensor Based on Crystalline Tin Oxide Nanoparticles Encapsulated in Polyaniline Matrix. *Microchim Acta* **2016**, *183* (2), 573−580.
(54) Qi, P.; Zhang, T.; Shao, J.; Yang, B.; Fei, T.; Wang, R. A QCM Humidity Sensor Constructed by Graphene Quantum Dots and Chitosan Composites. *Sensors and Actuators A: Physical* **2019**, *287*, 93−101.
(55) Silva, S. B.; Batista, G. L.; Santin, C. K. Chitosan for Sensors and Electrochemical Applications. In *Chitin and Chitosan*; Broek, L. A. M., Boeriu, C. G., Eds.; Wiley, 2019; pp 461−476. DOI: 10.1002/9781119450467.ch18.
(56) Xu, Z.; Zhang, D.; Liu, X.; Yang, Y.; Wang, X.; Xue, Q. Self-Powered Multifunctional Monitoring and Analysis System Based on Dual-Triboelectric Nanogenerator and Chitosan/Activated Carbon Film Humidity Sensor. *Nano Energy* **2022**, *94*, 106881.
(57) Matlou, G. G.; Abrahamse, H. Hybrid Inorganic-Organic Core-Shell Nanodrug Systems in Targeted Photodynamic Therapy of Cancer. *Pharmaceutics* **2021**, *13* (11), 1773.
(58) Zhang, S.; Li, L.; Lu, Y.; Liu, D.; Zhang, J.; Hao, D.; Zhang, X.; Xiong, L.; Huang, J. Sensitive Humidity Sensors Based on Ionically Conductive Metal-Organic Frameworks for Breath Monitoring and Non-Contact Sensing. *Applied Materials Today* **2022**, *26*, 101391.

(59) Choi, S.-J.; Kim, I.-D.; Park, H. J. 2D Layered Mn and Ru Oxide Nanosheets for Real-Time Breath Humidity Monitoring. *Appl. Surf. Sci.* **2022**, *573*, 151481.
(60) Dai, J.; Zhao, H.; Lin, X.; Liu, S.; Liu, Y.; Liu, X.; Fei, T.; Zhang, T. Ultrafast Response Polyelectrolyte Humidity Sensor for Respiration Monitoring. *ACS Appl. Mater. Interfaces* **2019**, *11* (6), 6483−6490.
(61) Ullah, A.; Zulfiqar, M. H.; Khan, M. A.; Zubair, M.; Mehmood, M. Q.; Massoud, Y. Fast Response Facile Fabricated IDE-Based Ultra-Sensitive Humidity Sensor for Medical Applications. *ACS Omega* **2023**, *8* (19), 16842−16850.
(62) Li, T.; Zhao, T.; Tian, X.; Yuan, L.; Xue, X.; Wang, Z.; Yin, L.; Zhang, J. A High-Performance Humidity Sensor Based on Alkalized MXenes and Poly(Dopamine) for Touchless Sensing and Respiration Monitoring. *J. Mater. Chem. C* **2022**, *10* (6), 2281−2289.
(63) Safer, J. D. Thyroid Hormone Action on Skin. *Derm.-Endocrinol.* **2011**, *3* (3), 211−215.

https://doi.org/10.1021/acsomega.3c05244
ACS Omega 2023, 8, 39511−39522